

Mapping for nonlinear electron interaction with whistler-mode waves.

A. V. Artemyev,^{1, a)} A. I. Neishtadt,^{2, b)} and A. A. Vasiliev³

¹⁾*Institute of Geophysics and Planetary Physics, University of California, Los Angeles, USA.*

²⁾*Department of Mathematical Sciences, Loughborough University, Loughborough LE11 3TU, United Kingdom.*

³⁾*Space Research Institute, RAS, Moscow, Russia.*

(Dated: 27 November 2019)

The resonant interaction of relativistic electrons and whistler waves is an important mechanism of electron acceleration and scattering in the Earth radiation belts and other space plasma systems. For low amplitude waves, such an interaction is well described by the quasi-linear diffusion theory, whereas nonlinear resonant effects induced by high-amplitude waves are mostly investigated (analytically and numerically) using the test particle approach. In this paper, we develop a mapping technique for the description of this nonlinear resonant interaction. Using the Hamiltonian theory for resonant systems, we derive the main characteristics of electron transport in the phase space and combine these characteristics to construct the map. This map can be considered as a generalization of the classical Chirikov map for systems with nondiffusive particle transport and allows us to model the long-term evolution of the electron distribution function.

I. INTRODUCTION

Whistler waves are electromagnetic emissions within the frequency range from the lower-hybrid up to electron cyclotron frequency widely observed in space^{1,46,80,94,96} and laboratory^{69,83} plasmas. These waves are generated by various types of electron distributions with thermal anisotropy^{38,87}, beam distributions^{8,42,91,92}, or both^{9,48,51}, and they play an important role in the isotropisation of originally unstable electron distributions^{29,44,74}. A classical theory of whistler wave resonant interaction with electrons is the quasi-linear theory^{37,45,88} that assumes a broad spectrum of low amplitude waves. This theory allows to describe the main characteristics of electron acceleration^{47,77} and scattering^{57,78} in the Earth radiation belts, in the solar wind⁶⁴, and at the Earth bow shock^{89,90}. However, quasi-linear theory cannot describe resonant interactions with the very intense coherent waves^{33,72} often observed in space plasmas^{2,79,81,93,94,97,98}. Such sufficiently intense whistlers can resonate nonlinearly with electrons^{21,34,58}. Such nonlinear interaction can lead to phase trapping or non-diffusive scattering of particles^{5,68} and can result in a very fast electron acceleration^{6,25,26,28,60,73,95}. Therefore, the effects of nonlinear resonant interaction are actively investigated (see reviews in Refs. 7, 9, 11, 61, and 66).

Since self-consistent Vlasov or Particle-In-Cell simulations of whistler wave generation and their resonances with electrons^{27,35,43,75} can hardly cover the long-term dynamics of the electron distribution in realistic space plasma systems, alternative approaches need to be considered. Beside the test particle approach (i.e., the numerical integration of a large number of electron trajectories^{3,41,59}), the most interesting approach

for the investigation of nonlinear electron resonances with whistler waves consists in the derivation of a kinetic equation (master-equation⁸⁴) describing the evolution of the electron distribution. This approach generalizes the quasi-linear diffusion equation by including terms responsible for electron nonlinear acceleration and scattering^{13,18,28,62}. Such terms can be derived analytically^{15,82} or numerically^{30,31,62}.

A less investigated but potentially useful approach is the mapping technique already widely used for systems with small wave amplitudes^{49,63}. The well-known Chirikov map²⁴ describes phase space diffusion and transport induced by periodical random jumps of particle momentum. The resonance of electrons and whistler waves results in a similar type of dynamics: each resonant interaction corresponds to an electron energy (and pitch-angle) jump inducing particle transport in phase space. For small amplitude whistler waves, the map of electron resonant jumps is quite similar to the Chirikov map^{39,40}, but nonlinear resonant interaction should significantly change such a map. In this study, we develop a map describing electron motion in a system with multiple passages through nonlinear resonances. We have also demonstrated that this map models well the electron distribution evolution and can be used to study the radiation belt dynamics.

II. BASIC EQUATIONS

To derive the basic properties of the nonlinear electron (m_e is the rest mass and $-e$ is the charge) interaction with field-aligned whistler waves (ω is a constant frequency, $k(\omega, s)$ is the wave number given by the cold plasma dispersion relation⁷⁰ and depending on the field-aligned coordinate s) we consider Hamiltonian (see de-

^{a)}Also at Space Research Institute, RAS, Moscow, Russia; Electronic mail: aartemyev@igpp.ucla.edu

^{b)}Also at Space Research Institute, RAS, Moscow, Russia

tails in, e.g., Refs. 16 and 82):

$$H = m_e c^2 \gamma + U_w(s, I_x) \sin(\phi + \psi)$$

$$\gamma = \sqrt{1 + \frac{p_{\parallel}^2}{m_e^2 c^2} + \frac{2I_x \Omega_{ce}}{m_e c^2}} \quad (1)$$

where c is the speed of light, γ is the gamma factor of the gyroaveraged system, $\Omega_{ce} = eB_0(s)/m_e c$ is the electron gyrofrequency in the background magnetic field $B_0(s)$ given by the reduced dipole model²¹, $U_w = \sqrt{2I_x \Omega_{ce} m_e e B_w / \gamma m_e c k}$ with B_w the wave amplitude, I_x is the magnetic moment normalized in a such a way that $I_x \Omega_{ce}$ has the dimension of energy. The conjugate pairs of variables in Eq. (1) are field-aligned coordinate and momentum, (s, p_{\parallel}) , and gyrophase and magnetic moment, ψ, I_x . Wave phase ϕ is given by the differential equation: $\dot{\phi} = k(s)\dot{s} - \omega$ (we omit the argument ω in the function k). In system (1) phases ϕ, ψ change much faster than variables s, p_{\parallel}, I_x because wave frequency ω and gyrofrequency Ω_{ce} are much larger than the electron bounce frequency $\sim c/R$ where R is a spatial scale of $B_0(s)$ gradient. Therefore, the first small parameter of the system is $c/R\Omega_{ce} \ll 1$. The second small parameter of the system is $B_w/B_0 \ll 1$, and we consider sufficiently intense waves with $B_w/B_0 \geq c/R\Omega_{ce}$ (this condition is satisfied for a significant fraction of whistler waves observed in the Earth radiation belts, see Ref. 98).

Figure 1(a) shows several fragments of electron trajectories around the resonance $\dot{\phi} + \dot{\psi} = 0$ (with $\dot{\psi} = \partial H/\partial I_x \approx \Omega_{ce}/\gamma$): there are two main effects⁵⁶ – electron trapping into resonance with the energy increase $\Delta\gamma_{trap}$, and electron scattering on the resonance with the energy decrease $\Delta\gamma_{scat}$. We plan to construct a map describing the long-term evolution produced by these two processes.

We start with the determination of $\Delta\gamma_{trap}$, $\Delta\gamma_{scat}$ and their dependencies on particle characteristics. First, we use the generating function $W_1 = ((\int k(\tilde{s})d\tilde{s} - \omega t) + \psi)I + sP$ to introduce phase $\varphi = \phi + \psi$ and conjugate momentum I :

$$H_I = -\omega I + m_e c^2 \gamma + U_w(s, I) \sin \varphi$$

$$\gamma = \sqrt{1 + \frac{(P + kI)^2}{m_e^2 c^2} + \frac{2I \Omega_{ce}}{m_e c^2}} \quad (2)$$

Pairs of conjugate variables are (I, φ) and (s, P) . The resonance condition ($\dot{\varphi} = \partial H_I/\partial I = 0$) for Hamiltonian (2) defines the resonant momentum $I_R(s, P)$:

$$\frac{kI_R}{m_e c} = \sqrt{\frac{1 - (\Omega_{ce}/kc)^2 - 2(\Omega_{ce}P/km_e c^2)}{(kc/\omega)^2 - 1}}$$

$$- \frac{\Omega_{ce}}{kc} - \frac{P}{m_e c} \quad (3)$$

We expand Hamiltonian (2) around the resonance

$$H_I \approx \Lambda + \frac{1}{2}g(I - I_R)^2 + U_w(s, I_R) \sin \varphi \quad (4)$$

$$\Lambda = -\omega I_R + m_e c^2 \gamma_R, \quad \gamma_R = \sqrt{1 + \frac{(P + kI_R)^2}{m_e^2 c^2} + \frac{2I_R \Omega_{ce}}{m_e c^2}}$$

$$g = m_e c^2 \left. \frac{\partial^2 \gamma}{\partial I^2} \right|_{I=I_R} = \frac{\omega^2 \left((kc/\omega)^2 - 1 \right)}{\gamma_R}$$

and use the generating function $W_2 = (I - I_R)\zeta + Ps^*$ to introduce new pairs of conjugate variables (ζ, P_{ζ}) and (s^*, P^*) with $s^* = s + (\partial I_R/\partial P)\zeta$, $P^* = P - (\partial I_R/\partial s)\zeta$:

$$\tilde{H}_I = \Lambda(s^*, P^*) + \frac{1}{2}gP_{\zeta}^2 + U_w(s, I_R) \sin \zeta$$

$$\approx \Lambda(s, P) + \frac{1}{2}gP_{\zeta}^2 - r\zeta + U_w(s, I_R) \sin \zeta$$

$$r = \{\Lambda, I_R\}_{s, P} = \frac{\partial \Lambda}{\partial s} \frac{\partial I_R}{\partial P} - \frac{\partial \Lambda}{\partial P} \frac{\partial I_R}{\partial s} \quad (5)$$

Using Hamiltonian (2), we get $m_e c^2 \Delta\gamma = \omega \Delta I$ (note $\partial H_I/\partial t = 0$) and $\dot{I} = -\partial H_I/\partial \varphi = -U_w \cos(\varphi)$. Therefore, the energy change $\Delta\gamma$ due to resonant interaction can be written as^{11,55}

$$m_e c^2 \Delta\gamma = -\omega U_w \int_{-\infty}^{+\infty} \cos \varphi dt = -2\omega U_w \int_{-\infty}^{t_R} \cos \varphi dt$$

$$= -2\omega U_w \int_{\zeta_R}^{+\infty} \frac{\cos \zeta}{gP_{\zeta}} d\zeta = -\sqrt{\frac{2}{g}} \omega \int_{\zeta_R}^{+\infty} \frac{U_w \cos \zeta d\zeta}{\sqrt{h_{\zeta} + r\zeta - U_w \sin \zeta}}$$

$$= -\sqrt{\frac{2U_w}{g}} \omega \int_{\zeta_R}^{+\infty} \frac{a \cos \zeta d\zeta}{\sqrt{(\zeta - \zeta_R) - a(\sin \zeta - \sin \zeta_R)}}$$

$$= -\sqrt{\frac{2r}{g}} \omega f(\zeta_R, a) \quad (6)$$

where t_R is the time of the resonant interaction, ζ_R is the value of ζ at $t = t_R$, and we use the Hamiltonian equation $\dot{\zeta} = \partial \tilde{H}_I/\partial P_{\zeta}$ to express P_{ζ} through the energy at the resonance $h_{\zeta} = \tilde{H}_I - \Lambda = U_w \sin \zeta_R - r\zeta_R$ (note Eq. (6) is written for $r > 0$, see details in Refs. 11 and 55). Coefficient $a = U_w/r$ determines the mode of resonant interaction: for $|a| > 1$ we deal with nonlinear interaction with $\langle \Delta\gamma \rangle_{h_{\zeta}} \neq 0$. Function $f(\zeta_R, a)$ is shown in Fig. 2 (a). This is a periodic function with the average value^{11,55} equal to

$$\langle \Delta\gamma \rangle_{h_{\zeta}} = \frac{\omega}{\pi} \sqrt{\frac{2r}{g}} \int_{\zeta_-}^{\zeta_+} \sqrt{(\zeta - \zeta_-) - a(\sin \zeta - \sin \zeta_-)} d\zeta \quad (7)$$

where ζ_{\pm} are shown in the phase portrait of $\tilde{H}_I - \Lambda$ Hamiltonian (see Fig. 1(b)).

The energy change in Eq. (7) represents the amplitude of energy scattering $\Delta\gamma_{scat} = \langle \Delta\gamma \rangle_{h_{\zeta}}$ and depends on the

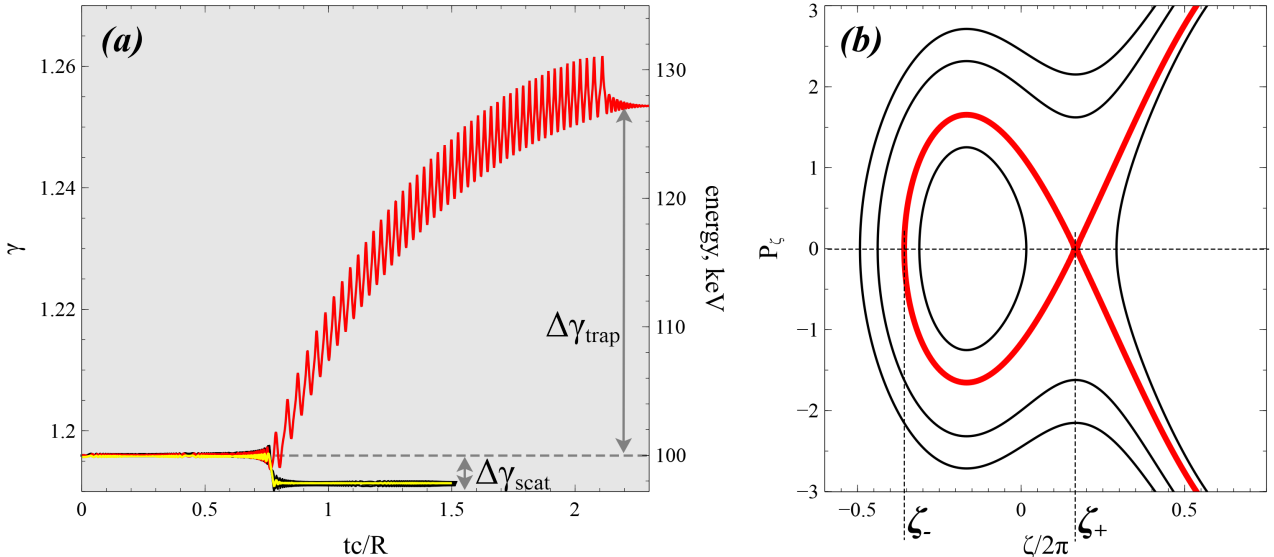


FIG. 1: (a) Change of electron energy due scattering (black; yellow shows averaged energy of scattered particle) and trapping (red). The time interval of one resonant interaction is shown. All electrons have initially the same energy and pitch-angle. For these trajectories and throughout the paper we consider a curvature-free dipole magnetic field²¹ with the radial distance from the Earth $R = 4.5$ of the Earth radii. The whistler wave frequency is 0.35 times the electron cyclotron frequency at the equator, and plasma frequency equals to 4.5 of the electron cyclotron frequency at the equator. To evaluate the wave number k we use the cold plasma dispersion of whistler waves⁷⁰. Wave amplitude is 300 pT, typical for intense whistlers observed in the radiation belts^{23,81,93,97}. The distribution of the wave amplitude along magnetic field lines, $B_w(s)$, is modeled by function $\tanh((\lambda/\delta\lambda_1)^2) \exp(-(\lambda/\delta\lambda_2)^2)$ with λ the magnetic latitude ($ds = Rd\lambda\sqrt{1 + \sin^2 \lambda \cos \lambda}$) and $\delta\lambda_1 = 2^\circ$, $\delta\lambda_2 = 20^\circ$. This function fits the observed whistler wave intensity distribution¹. To simplify the simulations, we consider waves in only one hemisphere, $B_w = 0$ for $s < 0$, and thus there is only one resonance for electrons within one bounce period. Waves are moving away from the equatorial plane, $s = 0$, to large s , i.e. only $k > 0$ are included. (b) Phase portrait of Hamiltonian

$$\tilde{H}_I - \Lambda = gP_\zeta^2/2 - r\zeta + U_w \sin \zeta \text{ for } |U_w/r| > 1.$$

resonance position s_R given by equations

$$h = -\omega I_R(s, P) + m_e c^2 \gamma_R(s, P), \quad \gamma_0 = \gamma_R(s, P) \quad (8)$$

where $m_e c^2 \gamma_0$ being the initial electron energy and $h = -\omega I_{x0} + m_e c^2 \gamma_0$ (with I_{x0} is the initial I_x value). Equations (8) can be rewritten as

$$\gamma_R = \left| \frac{\Omega_{ce}}{kc} \mp \frac{kc}{\sqrt{(kc)^2 - \omega^2}} \sqrt{1 + \left(\frac{\Omega_{ce}}{kc} \right)^2} - \frac{2h}{m_e c^2} \frac{\Omega_{ce}}{kc} \right| \quad (9)$$

Figure 2(b) shows $\Delta\gamma_{scat}(s_R)$. For a given h (or equivalently for a given initial pitch-angle α_0 determining I_{x0}) we can plot $\Delta\gamma_{scat}$ as a function of initial energy $m_e c^2 \gamma_0$, see Figure 2(c). As h is determined by α_0 and γ_0 , the amplitude of energy scattering $m_e c^2 \Delta\gamma_{scat}$ depends on α_0, γ_0 . Analogous dependencies of scattering amplitude on initial particle parameters has been tested for several specific Hamiltonians^{15,19,82}. For Hamiltonian (1) we compare the numerically calculated $\Delta\gamma_{scat}$ with the analytical expression (7) in Fig. 2(c): to evaluate $\Delta\gamma_{scat}$ numerically, for several γ_0 we run 10^4 trajectories for Hamiltonian (1) for fixed h and different γ_0 (the time of

integration of each trajectory includes only one resonant interaction) and then average energy changes.

In contrast to scattering, particle trapping is a non-local process. The energy change due to trapping significantly exceeds $\Delta\gamma_{scat}$ and can be comparable with the initial particle energy. Particles can be trapped if the probability of trapping Π is positive^{11,56}. For system (5), this probability is defined by the relation²⁰:

$$\Pi = -\frac{m_e c^2}{\omega} \frac{d\Delta\gamma_{scat}}{dI} = -\frac{m_e c^2}{\omega} \{\Delta\gamma_{scat}, I_R\} \quad (10)$$

where $\{\cdot, \cdot\}$ is the Poisson bracket with respect to the variables s, P . The value Π depends on the initial energy γ_0 and I_x in terms of their combination $h = -\omega I_{x0} + m_e c^2 \gamma_0$. If Eq. (10) gives a negative value, Π should be set to be zero and there are no trapped particles.

Equation (10) determines the relative number of resonant particles that get trapped during a single resonant interaction. Analogous equations have been verified using the test particle calculations for several specific Hamiltonians in Refs. 15, 20, and 82. Note that due to conservation of h , the change of I is equal to the change of $\gamma m_e c^2 / \omega$, and thus Eq. (10) can be written

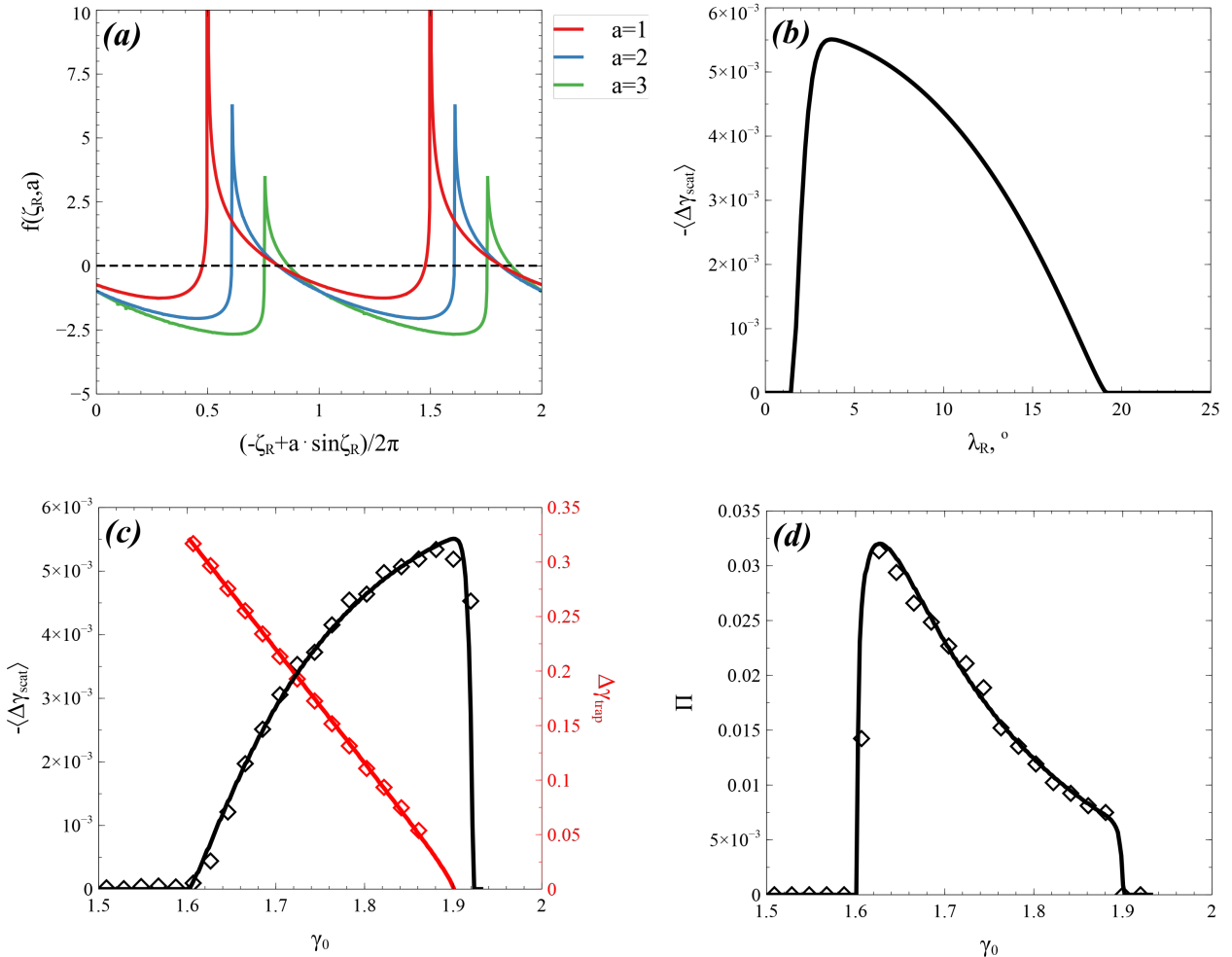


FIG. 2: Main parameters of the resonant system: (a) function $f(\zeta_R, a)$; (b) function $\langle \Delta\gamma_{scat}(\lambda_R) \rangle$, (c) function $\langle \Delta\gamma_{scat}(\gamma_0) \rangle$; (d) probability of trapping $\Pi(\gamma_0)$. Symbols show the results of numerical simulations ($h/m_e c^2 = 1.454$ corresponds to, e.g., $\alpha_0 = 45^\circ$ of the equatorial pitch-angle for 300 keV electron energy; see details of model parameters in the caption of Fig. 1).

as $\Pi = -d\Delta\gamma_{scat}/d\gamma$, i.e. the derivative of the profile $\Delta\gamma_{scat}(\gamma)$ from Fig. 2(c) should give the $\Pi(\gamma)$ profile (for fixed h). Figure 2(d) shows this $\Pi(\gamma)$ and the corresponding numerical verifications (each numerical point shows the relative number of 10^4 particles that have been trapped during the first resonant interaction).

Being trapped at some resonant value s_R defined by Eqs. (8), particles should escape at s_{detrap} with an energy gain $\Delta\gamma_{trap} = \gamma_R(s_{detrap}) - \gamma_0$. This detrappping coordinate can be calculated using the conservation of the adiabatic invariant $(2\pi)^{-1} \oint P_\zeta d\zeta$ for trapped particles (see details in, e.g., Refs. 15 and 82). Formally speaking, s_{detrap} is the solution of equation $\Delta\gamma_{scat}(s_{detrap}) = \Delta\gamma_{scat}(s_R)$, i.e., the function (7) should have the same value at the trapping and detrappping positions^{20,85}.

To summarize, for a given $h = -\omega I_{x0} + \gamma_0 m_e c^2$, the resonant system (1) can be reduced to a 1D system that is described by the profile of energy change

due to scattering $\Delta\gamma_{scat}(\gamma)$, probability of trapping $\Pi = \max(0, -d\Delta\gamma_{scat}/d\gamma)$, and energy change due to trapping $\Delta\gamma_{trap}(\gamma)$. These three functions allow us to construct a map describing the system evolution on a time interval including many resonances.

III. MAPPING TECHNIQUE

Let us discuss the meaning of the probability of trapping, Π . Each trajectory far from the resonance is characterized by initial energy γ , magnetic moment I_x , coordinates in the (s, p_\parallel) plane, and phase ζ which coincides with φ . Knowing these values we can determine if particles will be trapped or scattered during the first resonant interaction. However, particle phase ζ changes with time much faster than particle s, p_\parallel coordinates ($\dot{\zeta} \sim \Omega_{ce}$ is

the largest frequency in the system). Therefore, even a small initial variation of ζ can result in a crucial change of the particle's fate: trapped particles may become scattered and vice versa. Accordingly, instead of tracing individual trajectories with given ζ , it is more suitable to adopt a probabilistic approach and to consider the relative amount of trapped particle trajectories, equal to Π (see Refs. 54 and 65).

Will a particle be trapped or scattered depends on ζ value at the resonance, ζ_R , but instead of ζ it is more convenient to use the normalized resonant energy $\xi = (a \sin \zeta_R - \zeta_R)/2\pi - (a \sin \zeta_+ - \zeta_+)/2\pi$ (where $\zeta_R \in [\zeta_+ - 2\pi, \zeta_-]$, see Fig. 1(b)), which is distributed uniformly (see numerical tests of ξ distributions in, e.g., Refs. 17 and 32); its values belong to the interval $[0, 1]$. Within this interval, the measure of the sub-range corresponding to trapping equals Π , and we can assume for simplicity that this sub-range is $0 \leq \xi \leq \Pi$. As the particle energy does not change between two successive resonant interactions, we can write a map of the $\gamma \rightarrow \bar{\gamma}$ transition during a single resonance:

$$\begin{aligned} \bar{\gamma} &= \gamma + \begin{cases} \Delta\gamma_{trap}(\gamma), & \xi \in [0, \Pi] \\ \Delta\gamma_{scat}(\gamma), & \xi \in (\Pi, 1] \end{cases} \\ \Pi &= -d\Delta\gamma_{scat}/d\gamma \end{aligned} \quad (11)$$

The map (11) should be supplemented with a map for phase ξ , which is related to ζ change (gain) between two resonances through the equation (see Appendix A):

$$\bar{\xi} = \xi - \Delta\zeta/2\pi \quad (12)$$

The rate of ζ change is defined by the Hamiltonian system (2) (note that $\zeta = \varphi$), but it is more convenient to use notations of the Hamiltonian system (1):

$$\begin{aligned} \dot{\zeta} &= -\omega + \frac{\Omega_{ce}(s)}{\gamma} + k(s) \frac{p_{\parallel}}{m_e \gamma} \\ p_{\parallel} &= m_e c \sqrt{\gamma^2 - 1 - \frac{2I_x \Omega_{ce}(s)}{m_e c^2}} \end{aligned} \quad (13)$$

Integrating Eq. (13) over the time interval between two resonances (in the system under consideration this time is equal to the bounce period τ_b), we obtain

$$\begin{aligned} \Delta\zeta &= \omega\tau_b \left(\frac{\varpi}{\gamma} - 1 \right) \\ \tau_b &= \frac{4}{c} \int_0^{s_{\max}} \left(\gamma^2 - 1 - \frac{2I_x \Omega_{ce}(s)}{m_e c^2} \right)^{-1/2} ds \\ \varpi &= \frac{\int_0^{s_{\max}} \Omega_{ce}(s) \left(\gamma^2 - 1 - \frac{2I_x \Omega_{ce}(s)}{m_e c^2} \right)^{-1/2} ds}{\int_0^{s_{\max}} \omega \left(\gamma^2 - 1 - \frac{2I_x \Omega_{ce}(s)}{m_e c^2} \right)^{-1/2} ds} \end{aligned} \quad (14)$$

where τ_b and ϖ depend on energy γ and I_x or, at h fixed, these functions depend only on γ (see Fig. 3). Note that the integral $\gamma^{-1} \oint k(s)p_{\parallel} dt = \oint k(s)ds$ is equal to zero.

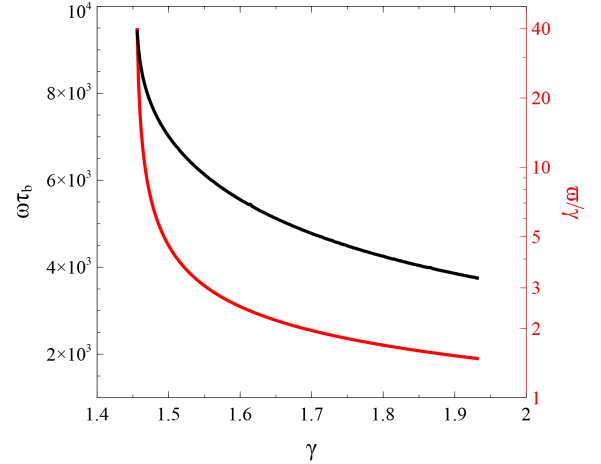


FIG. 3: Functions $\omega\tau_b(\gamma)$, $\varpi(\gamma)$ for fixed value of h ($h/m_ec^2 = 1.454$ corresponding, e.g., to an equatorial pitch-angle $\alpha_0 = 45^\circ$ for a 300 keV electron; see details of model parameters in the caption of Fig. 1).

Combining Eq. (14) and Eq. (11), we obtain the map for this resonant system in the (γ, ζ) plane:

$$\begin{aligned} \bar{\xi} &= \xi - \omega\tau_b(\varpi\gamma^{-1} - 1)/2\pi, \quad \Pi = -d\Delta\gamma_{scat}/d\gamma \\ \bar{\gamma} &= \gamma + \begin{cases} \Delta\gamma_{trap}(\gamma), & \bar{\xi} \in [0, \Pi] \\ \Delta\gamma_{scat}(\gamma), & \bar{\xi} \in (\Pi, 1] \end{cases} \end{aligned} \quad (15)$$

This map describes variation of particle energy and phase. Figure 4(a) shows a typical trajectory obtained from 200 iterations for map (15): the particle loses energy due to scattering and sometimes (when the phase appears to be within the short range $[0, \Pi]$) gains energy due to trapping. After a sufficiently large number of iterations, the particle trajectory fills the entire (ζ, γ) plane (within the range of the resonant energies for which $\Delta\gamma_{scat} \neq 0$), as shown in Fig. 4(b). Such spreading of a single trajectory means that any initial distribution of energy should tend toward a uniform distribution (note that we are speaking of energies for a fixed h , i.e. the energy distribution along the resonant curve^{50,71}). A similar result has been obtained through numerical simulations and solutions⁵³ of the kinetic equation¹³ describing the long-term dynamics of a system consisting of many trajectories (1). In the next section, to check the derived map (15), we compare the results provided by this map with results of test particle simulations, as well as with results obtained by solving the full kinetic equation.

IV. VERIFICATION OF MAPPING RESULTS

Let us fix h and consider a 1D energy distribution $\Psi(\gamma)$ (note that Ψ is a cut of the 2D energy/pitch-angle distribution). We can represent this distribution as a set of 10^6 individual particles with different initial energies and randomly distributed phases. Then, the trajectory

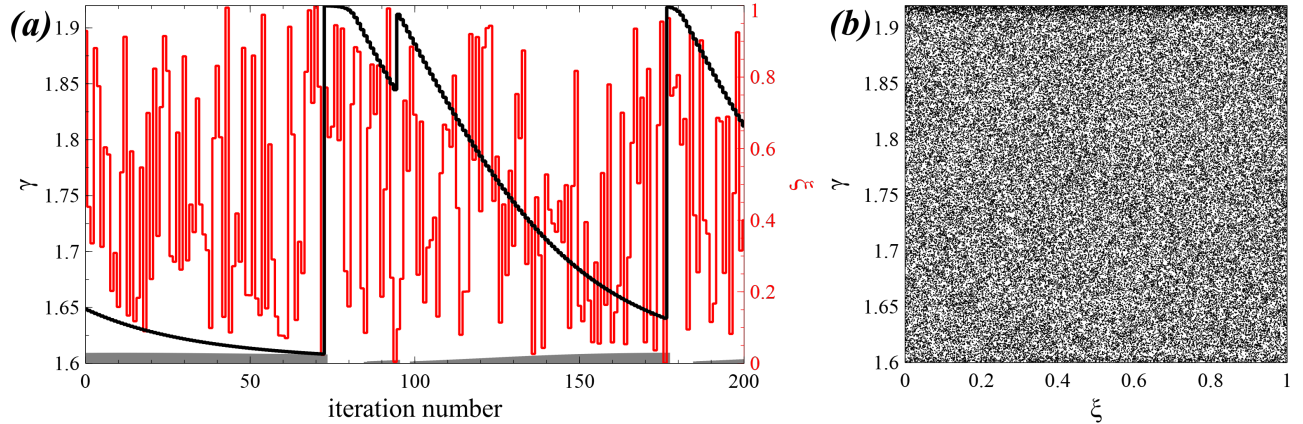


FIG. 4: (a) Particle trajectory for map (15): γ and ξ as functions of iteration number, grey color shows the capture probability Π . (b) Particle trajectory in (h_R, γ) plane for 10^5 iterations. ($h/m_ec^2 = 1.454$ corresponds to, e.g., $\alpha_0 = 45^\circ$ of the equatorial pitch-angle for 300 keV electron energy; see details of model parameters in the caption of Fig. 1).

of each particle can be traced numerically using Hamiltonian equations (1) over a time interval including many resonance interactions. This method reproduces the evolution of $\Psi(\gamma)$ driven by the wave-particle resonant interaction. Alternatively, we can trace trajectories and reproduce the evolution of $\Psi(\gamma)$ using the map (15). The third approach is to solve the kinetic equation that describes Ψ evolution due to nonlinear resonant interactions^{13,16}:

$$\frac{\partial \Psi}{\partial t} = V \frac{\partial \Psi}{\partial J} + \frac{dV}{dJ} (\Psi^* - \Psi) \Theta(J) \quad (16)$$

where $J(\gamma) = \int^\gamma \tau_b(\gamma') d\gamma'$, $V = \Delta\gamma_{scat}/\tau_b$, $\Psi^* = \Psi(\gamma^*)$ with $\gamma^* + \Delta\gamma_{trap}(\gamma^*) = \gamma$, and $\Theta = 0$ for $\Pi = 0$ and $\Theta = 1$ for $\Pi > 0$. Equation (16) can be re-written in a simplified form

$$\frac{\partial \Psi}{\partial t} = V \frac{\partial \Psi}{\partial \gamma} + \frac{dV}{d\gamma} (\Psi^* \tau_b(\gamma^*)/\tau_b(\gamma) - \Psi) \Theta(\gamma) + \ell \quad (17)$$

where the term ℓ includes derivatives $\sim \partial\tau_b/\partial\gamma$ and can be omitted for a sufficiently weak $\tau_b(\gamma)$ dependence (see details of $\gamma \rightarrow J(\gamma)$ transformation in Refs. 14 and 16).

We consider such three types of solutions of $\Psi(\gamma)$ evolution (test particles, Eq. (16), and map (15)) for two initial distributions Ψ . Figure 5 shows these three solutions for initial power law energy distribution and three moments of time (note that solutions obtained via test particle simulations and Eq. (16) depend on time, whereas the map (15) depends on the iteration number that should be transformed to time using the bounce period $\tau_b(\gamma)$ for each trajectory). All three solutions show a very similar evolution of $\Psi(\gamma)$: the distribution gets flattened within the resonant energy range (where $\Delta\gamma_{scat} \neq 0$) and forms a plateau. This is the effect of a competition between trapping (energy increase) and scattering (energy decrease), that ultimately results in a uniform distribution (note that this uniform distribution is formed along the resonance curves^{50,71}, i.e. for $h = \text{const}$). A similar evolution, although more complicated, can be seen in

Fig. 6 showing three solutions for an initial $\Psi(\gamma)$ with a local maximum. This maximum starts drifting to lower energies (due to scattering), whereas a new maximum forms at high energies (due to trapping acceleration). Finally $\Psi(\gamma)$ will be flattened and form a plateau within the resonant energy range. Such an evolution of $\Psi(\gamma)$ has been predicted and described (considering solutions of Eq. (16)) in Refs. 10 and 53.

V. DISCUSSION

In this study, we have developed a map describing the dynamics of systems with nonlinear resonant wave-particle interactions. For illustration we used wave and background plasma parameters typical for the Earth inner magnetosphere, where relativistic electrons resonate with high amplitude whistlers. This system is well investigated in the regime of low wave amplitudes where quasi-linear diffusion equations are applicable^{50,67,76}, but so far there is no method allowing to model the long-term evolution of this system in the presence of nonlinear resonant effects. One of the most widespread technique, test particle simulation^{4,22,25,26,36,52,60}, provides a lot of important information about electron acceleration and scattering rates, but such simulations are limited to quite short time intervals. This limitation mostly comes from the need to integrate the entire (bounce) particle trajectory even if energy and magnetic moment only change at the locations of wave-particle resonances. Therefore, a natural solution consists in considering only resonance-induced changes of particle energy and pitch-angle, like in the quasi-linear diffusion approach. The generalization of the diffusion equation with inclusion of terms related to nonlinear wave-particle interaction results in Eq. (16) or similar types of kinetic equations^{13,16,68}. However, this kinetic equation still relies on the assumption of a

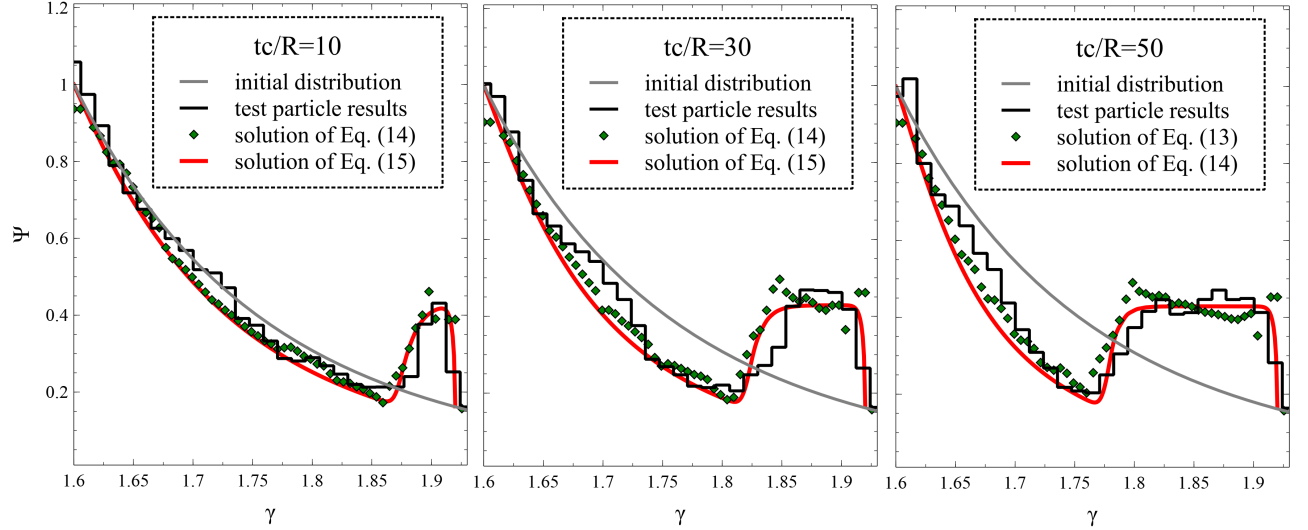


FIG. 5: Evolution of distribution $\Psi(\gamma)$ for $h/m_ec^2 = 1.454$ (this value of h corresponds to, e.g., equatorial pitch-angle $\alpha_0 = 45^\circ$ for 300 keV electron energy; see details of the model parameters in the caption to Fig. 1): black color shows results of test particle simulations (10^6 trajectories), red color shows solutions of Eq. (16), green color shows results of mapping (15). The initial distribution $\Psi(\gamma)$ is shown in all panels with grey curves. Time is normalized on R/c (a scale of the quarter of the bounce period) with $R = 4.5$ Earth radii.

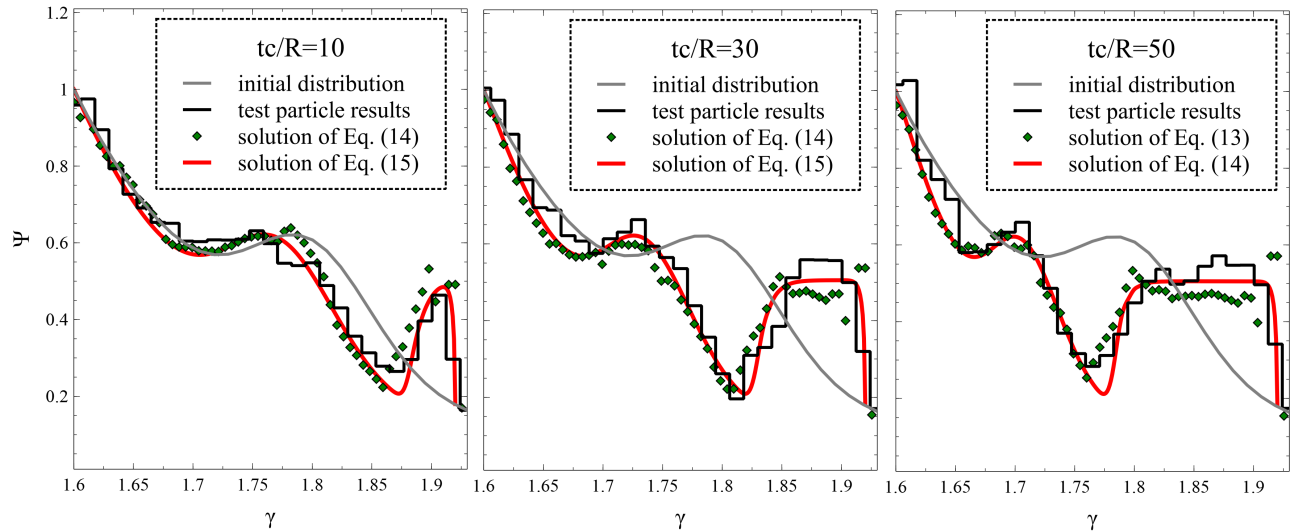


FIG. 6: Evolution of the distribution $\Psi(\gamma)$ for $h/m_ec^2 = 1.454$ (this value of h corresponds to, e.g., equatorial pitch-angle $\alpha_0 = 45^\circ$ for 300 keV electron energy; see details of the model parameters in the caption of Fig. 1): black color shows results of test particle simulations (10^6 trajectories), red color shows solutions of Eq. (16), green color shows results of mapping (15). The initial distribution $\Psi(\gamma)$ is shown in all panels with grey curves. Time is normalized to R/c (the quarter of the bounce period) with $R = 4.5$ Earth radii.

uniform distribution of resonant phases (i.e., it excludes effects related to phase correlation at multiple passages through the resonance) and it cannot be easily generalized for systems with multiple waves. These two problems can be resolved using the map approach that includes resonant phase dynamics while also allowing the inclusion of many resonances. Let us consider these two issues in more details.

Assuming a uniform distribution of resonant phases corresponds to the assumption that two successive resonances are not correlated, i.e., that electron energy jumps $\Delta\gamma$ (due to trapping or scattering) can be considered as independent over a long run. This important property of the resonant system usually results from the dependence of the phase gain $\Delta\zeta$ on energy γ (see Eq. (15)). This gain is usually large $\Delta\zeta \sim \omega\tau_b \gg 1$ (since whistler wave

period is much smaller than the electron bounce period along magnetic field lines) and, thus, even a small change of energy $\Delta\gamma$ due to resonant interaction should result in a significant change of $\Delta\zeta$: $\delta(\Delta\zeta) \sim (\partial\Delta\zeta/\partial\gamma)\Delta\gamma$, justifying the assumption of randomly distributed phases. However, resonances can be correlated (and the distribution of resonant phases can be non-uniform, see Ref. 12) for systems with small $\partial\Delta\zeta/\partial\gamma$. Such a situation can hardly appear in the Earth radiation belts, but it is more realistic for resonant electron interaction with strong electrostatic waves and solitons around the bow shock⁸⁶. This corresponds to Landau resonant interaction without the term ϖ/γ in Eq. (15) and with the time interval between resonances $\sim\tau_b$ weakly depending on energy. Therefore, the proposed map technique may be useful for investigations of nonlinear wave-particle interactions in such systems, where the assumption of a uniform distribution of resonant phases is not applicable.

The map (15) has been constructed for a system with a single wave (single resonance). In this system the condition $h = \text{const}$ reduces the initially 2D space (energy/pitch-angle or (γ, I_x)) to 1D space. However, unlike kinetic equation (16), this map can be generalized to many resonances resulting in particle motion in the (γ, I_x) space. Indeed, the map describes change of the resonant phase ζ between two resonances and energy change on the resonance. The ζ change can be modified by replacing the integration over the entire bounce period with the integration between two resonances in Eq. (14), whereas the energy change can be replaced with energy and I_x changes. This generalization looks much simpler to achieve than the corresponding generalization of the kinetic equation (16).

Figure 4 shows that after many iterations the particle trajectory fills the entire available space in the (ζ, γ) space. For ensembles including many trajectories, the final state of the distribution function will be a uniform distribution where phase space density Ψ should have the same value for all energies. This is the final state for both quasi-linear diffusion, that tends to reduce gradients of Ψ along the resonance curve, and nonlinear wave-particle interaction described by Eq. (16), which has only one stationary solution $\Psi = \text{const}$ (see Ref. 10). Therefore, the map (15) describes distribution flattening, $\partial\Psi/\partial\gamma \rightarrow 0$, and allows to estimate a typical timescale of this flattening. For example, Fig. 7 shows the evolution of the dispersion $D = \sqrt{\langle\gamma^2\rangle - \langle\gamma\rangle^2}$ of distribution Ψ for four different initial Ψ (shown in the inserted panel). The dynamics of Ψ is described by 10^5 trajectories of map (15), and D is normalized to the dispersion of the uniform distribution for the same γ range (i.e., $D/D_0 \approx 1$ means $\Psi \approx \text{const}$). As the map (15) describes discrete changes of energy with time, the beginning of the D evolution consists of step-like jumps (note that we transformed the iteration number to time for each trajectory to plot D versus time). Independently of the initial distribution, $D/D_0 \approx 1$ after $\approx 100\tau_b$, and this timescale is much

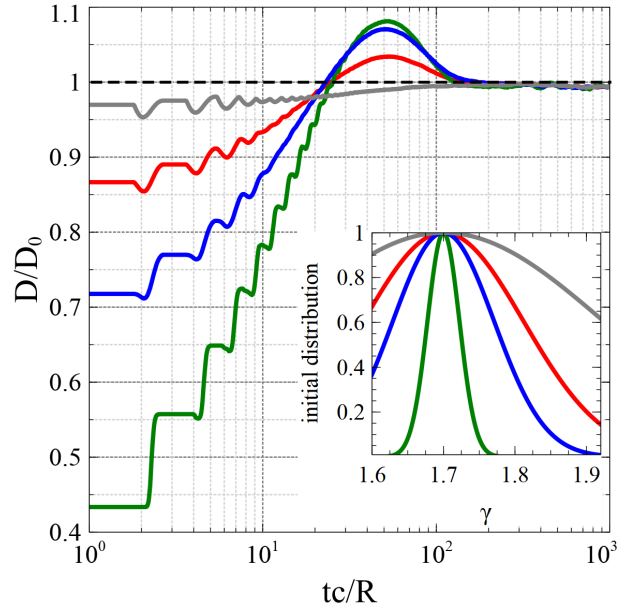


FIG. 7: Evolution of dispersion $D = \sqrt{\langle\gamma^2\rangle - \langle\gamma\rangle^2}$ for four distributions $\Psi(\gamma)$ and $h/m_{ec}^2 = 1.454$ (this value of h corresponds to, e.g. 45° of the equatorial pitch-angle for 300 keV electron energy; see details of model parameters in the caption of Fig. 1). Dispersions are normalized to the dispersion D_0 of the uniform distribution $\Psi = \text{const}$.

shorter than typical quasi-linear time scales^{47,77}.

To conclude, in this paper we have considered nonlinear resonances between relativistic electrons and intense whistler-mode waves. We have demonstrated that the long-term dynamics of the electron distribution can be described by a map taking into account the important interdependence between the probability of trapping Π and energy change due to scattering $\Delta\gamma_{scat}$: $\Pi = -d\Delta\gamma_{scat}/d\gamma$. This map is different from the classical Chirikov map²⁴, and allows to describe both effects of phase trapping and nonlinear scattering. The proposed mapping technique can be useful for the description of charged particle acceleration in various space plasma systems including the Earth radiation belts and the Earth bow shock.

ACKNOWLEDGMENTS

Authors are grateful to Dr. D. Mourenas for useful discussion. This work was supported by the Russian Scientific Fund, project 19-12-00313.

APPENDIX A

In this Appendix we derive the relation between h_R change between two resonance crossings and phase ζ gain

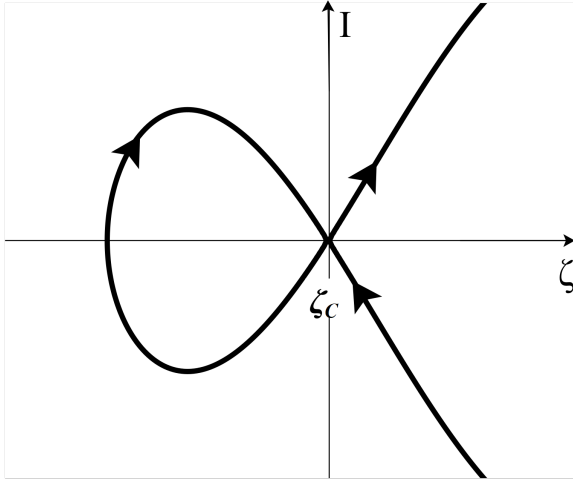


FIG. 8: Schematic of phase portrait.

between these crossings. We consider quite general form of Hamiltonian, but results of our derivations are directly applicable to the particular system considered in the main text.

Let us consider a general Hamiltonian as a sum of unperturbed part $H_0(I, p, q)$ and small perturbation $\varepsilon H_1(I, \zeta, p, q)$ (with $\varepsilon \ll 1$) where $(q, \varepsilon^{-1}p)$, (ζ, I) are pairs of conjugate variables: hence (ζ, I) are fast variables, (q, p) are slow variables, and H_1 is periodic in ζ (note in the main text $\varepsilon \sim B_w/B_0$). Momentum I is the adiabatic invariant: I is constant in the unperturbed system $H = H_0$, whereas under the perturbation $\dot{I} = -\varepsilon \partial H_1 / \partial \zeta$. There is no explicit dependence on time, and thus $H = h = \text{const}$. The resonance condition is determined by the equation $\partial H_0 / \partial I = 0$ that gives $I = I_R(p, q)$. We introduce $\Lambda(p, q) = H_0(I_R(p, q), p, q)$ and the improved adiabatic invariant J with the variable transformation $(I, \zeta, p, q) \rightarrow (J, \theta, P, Q)$, such that new Hamiltonian is $H = H_0(J, P, Q) + \varepsilon \bar{H}_1(J, P, Q)$ (in the leading approximation) with $\bar{H}_1 = \langle H_1 \rangle_\zeta$ (note new $H = h = \text{const}$).

We consider the resonance surface $I = I_R$ and assume that near this surface the phase portrait of the original Hamiltonian looks like one shown in Fig. 8. Far from the resonance θ changes with the frequency

$$\dot{\theta} = \frac{\partial H_0}{\partial J} + \varepsilon \frac{\partial \bar{H}_1}{\partial J} \quad (18)$$

with $J = \text{const}$, and

$$\dot{Q} = \varepsilon \frac{\partial H_0}{\partial P} + \varepsilon^2 \frac{\partial \bar{H}_1}{\partial P}, \quad \dot{P} = -\varepsilon \frac{\partial H_0}{\partial Q} - \varepsilon^2 \frac{\partial \bar{H}_1}{\partial Q} \quad (19)$$

We introduce $\omega_0(J, P, Q) = \partial H_0 / \partial J$, $\omega_1(J, P, Q) = \partial \bar{H}_1 / \partial J$, and consider large number $N \gg 1$ of ζ rotations from $t = t_0$ (when phase point is far from the resonance and moves towards the resonance) to $t = t_N$; the last turn is sufficiently far from the resonance and $\theta \approx \zeta$ in

the leading approximation. The last turn ends at $\zeta = \zeta_c \bmod 2\pi$ (see Fig. 8 for ζ_c definition). Then

$$\zeta_{cN} + 2\pi N = \zeta_0 + \int_{t_0}^{t_N} (\omega_0 + \varepsilon \omega_1) dt \quad (20)$$

where ζ_{cN} is ζ_c value at $t = t_N$. We introduce t_* as the time of crossing the resonance, i.e. $\omega_0(J, P, Q)|_{t=t_*} = 0$ and rewrite Eq. (20):

$$\zeta_{cN} + 2\pi N = \zeta_0 + \int_{t_0}^{t_*} (\omega_0 + \varepsilon \omega_1) dt - \int_{t_N}^{t_*} (\omega_0 + \varepsilon \omega_1) dt \quad (21)$$

Because time interval $t_* - t_N \ll 1/\varepsilon$ we can use $\dot{Q} = \varepsilon \partial H_0 / \partial P$, $\dot{P} = -\varepsilon \partial H_0 / \partial P$ and $Q \approx q$, $P \approx p$ in the last integral in Eq. (21). We also assume that $\zeta_{cN} \approx \zeta_{c*} = \zeta_c|_{t=t_*}$. To describe system dynamics for $t \in [t_N, t_*]$ we use the expansion of the Hamiltonian around the resonance $H = \Lambda + F$ and

$$F = \frac{1}{2} g (I - I_R)^2 + \varepsilon H_1, \quad g = \left. \frac{\partial^2 H_0}{\partial I^2} \right|_{I=I_R} \approx \text{const} \quad (22)$$

The Hamiltonian in new variables (J, θ, P, Q) can be expanded as

$$H = \Lambda + \frac{1}{2} g (J - I_R)^2 + \varepsilon \bar{H}_1 \quad (23)$$

We introduce $\bar{e} = g(J - I_R)^2 / 2$ and write

$$\begin{aligned} \dot{\bar{e}} &= \varepsilon g (J - I_R) r, \quad r = -\{I_R, \Lambda\} \approx \text{const} \\ \omega_0 &= \frac{\partial H}{\partial J} = g (J - I_R) \end{aligned} \quad (24)$$

Using $dt = d\bar{e}/(\partial \bar{e} / \partial t)$ we rewrite integral

$$\int_{t_N}^{t_*} (\omega_0 + \varepsilon \omega_1) dt \approx \frac{1}{\varepsilon} \int_{\bar{e}_N}^0 \frac{\omega_0 d\bar{e}}{g (J - I_R) r} = \frac{1}{\varepsilon} \int_{\bar{e}_N}^0 \frac{d\bar{e}}{r} = -\frac{\bar{e}_N}{\varepsilon r} \quad (25)$$

where we take into account that $\bar{e}_* = 0$ (by definition) and omit $\varepsilon \omega_1$ because $t_* - t_N \ll 1/\varepsilon$. Using definition $\bar{e} + \varepsilon \bar{H}_1 = F$, we write

$$\bar{e}_N = F_N - \varepsilon \bar{H}_1 \approx F_N - \varepsilon \bar{H}_{1*} \quad (26)$$

where \bar{H}_{1*} is the resonant value of \bar{H}_1 . Substituting Eqs. (25, 26) to Eq. (21), we obtain

$$\zeta_{c*} + 2\pi N = \zeta_0 + \int_{t_0}^{t_*} (\omega_0 + \varepsilon \omega_1) dt + \frac{F_N - \varepsilon \bar{H}_{1*}}{r \varepsilon} \quad (27)$$

or

$$\frac{F_N}{2\pi r \varepsilon} = \frac{\bar{H}_{1*}}{2\pi r} - \frac{1}{2\pi} \left(\zeta_0 - \zeta_{c*} + \int_{t_0}^{t_*} (\omega_0 + \varepsilon \omega_1) dt \right) \bmod 1 \quad (28)$$

We define F_{last} as an F value at the last crossing $\zeta = \zeta_c$ before the resonance. Thus, $F_{last} = F_N \bmod 2\pi\varepsilon r$, because the change of F after one ζ rotation equals to $2\pi\varepsilon r$. We introduce $\xi = (F_{last} - \varepsilon H_{1c*})/(2\pi\varepsilon r)$ (where H_{1c*} equals to H_1 at $\zeta = \zeta_c$, $t = t_*$) and $\tau = \varepsilon t$, and write

$$\xi = \text{Frac} \left(\frac{\bar{H}_{1*} - H_{1c*}}{2\pi r} - \frac{\zeta_0 - \zeta_{c*}}{2\pi} - \int_{\tau_0}^{\tau_*} \frac{(\omega_0 + \varepsilon\omega_1)}{2\pi\varepsilon} d\tau \right) \quad (29)$$

Note that ξ can be written as

$$\begin{aligned} \xi &= \frac{F_{last} - \varepsilon H_{1c*}}{2\pi\varepsilon r} = \frac{F_{last} - \varepsilon r\zeta_{c*} - (\varepsilon H_{1c*} - \varepsilon r\zeta_{c*})}{2\pi\varepsilon r} \\ &= \frac{E_{last} - E_{c*}}{2\pi\varepsilon r} \end{aligned} \quad (30)$$

where

$$E = \frac{1}{2}g(I - I_R)^2 - \varepsilon r\zeta + \varepsilon H_1, \quad (31)$$

and E_{c*} is E value at $\zeta = \zeta_c$, $t = t_*$, E_{last} is E value at last crossing of $\zeta = \zeta_c$ before resonance. Therefore, change of ξ between two resonance crossings at moments τ_* and τ_{*+} equals to the difference $\Delta\xi = \xi(\tau_{*+}) - \xi(\tau_*)$ given by Eq. (29), i.e. ξ gain is

$$\Delta\xi = - \int_{\tau_*}^{\tau_{*+}} \frac{(\omega_0 + \varepsilon\omega_1)}{2\pi\varepsilon} d\tau,$$

and this is the phase ζ gain between two resonance crossings normalized on 2π (between moments τ_* and τ_{*+}) taken with the minus sign.

- ¹Agapitov, O., Artemyev, A., Krasnoselskikh, V., Khotyaintsev, Y.V., Mourenas, D., Breuillard, H., Balikhin, M., Rolland, G., 2013. J. Geophys. Res. 118, 3407–3420. doi:10.1002/jgra.50312.
- ²Agapitov, O., Artemyev, A., Mourenas, D., Krasnoselskikh, V., Bonnell, J., Le Contel, O., Cully, C.M., Angelopoulos, V., 2014. J. Geophys. Res. 119, 1606–1626. doi:10.1002/2013JA019223.
- ³Agapitov, O.V., Artemyev, A.V., Mourenas, D., Mozer, F.S., Krasnoselskikh, V., 2015. Geophys. Res. Lett. 42, 10. doi:10.1002/2015GL066887.
- ⁴Agapitov, O.V., Mourenas, D., Artemyev, A.V., Mozer, F.S., 2016. Geophys. Res. Lett. 43, 11,112–11,120. URL: <http://dx.doi.org/10.1002/2016GL071250>, doi:10.1002/2016GL071250.
- ⁵Albert, J.M., 1993. Physics of Fluids B 5, 2744–2750. doi:10.1063/1.860715.
- ⁶Albert, J.M., 2002. Geophys. Res. Lett. 29, 1275. doi:10.1029/2001GL013941.
- ⁷Albert, J.M., Tao, X., Bortnik, J., 2013. Aspects of Nonlinear Wave-Particle Interactions, in: Summers, D., Mann, I.U., Baker, D.N., Schulz, M. (Eds.), Dynamics of the Earth's Radiation Belts and Inner Magnetosphere. doi:10.1029/2012GM001324.
- ⁸An, X., Van Compernolle, B., Bortnik, J., Thorne, R.M., Chen, L., Li, W., 2016. Geophys. Res. Lett. 43, 2413–2421. doi:10.1002/2015GL067126.
- ⁹Artemyev, A., Agapitov, O., Mourenas, D., Krasnoselskikh, V., Shastun, V., Mozer, F., 2016. Space Science Reviews 200, 261–355. URL: <http://dx.doi.org/10.1007/s11214-016-0252-5>, doi:10.1007/s11214-016-0252-5.
- ¹⁰Artemyev, A., Neishtadt, A., Vasiliev, A., 2019. Physica D: Nonlinear Phenomena URL: <http://www.sciencedirect.com/science/article/pii/S0167278918304433>, doi: <https://doi.org/10.1016/j.physd.2018.12.007>.
- ¹¹Artemyev, A.V., Neishtadt, A.I., Vainchtein, D.L., Vasiliev, A.A., Vasko, I.Y., Zelenyi, L.M., 2018a. Communications in Nonlinear Science and Numerical Simulations 65, 111–160. doi:10.1016/j.cnsns.2018.05.004.
- ¹²Artemyev, A.V., Neishtadt, A.I., Vasiliev, A.A., 2019. arXiv e-prints, arXiv:1904.02973arXiv:1904.02973.
- ¹³Artemyev, A.V., Neishtadt, A.I., Vasiliev, A.A., Mourenas, D., 2016. Physics of Plasmas 23, 090701. doi:10.1063/1.4962526.
- ¹⁴Artemyev, A.V., Neishtadt, A.I., Vasiliev, A.A., Mourenas, D., 2017a. ArXiv e-prints arXiv:1710.04489.
- ¹⁵Artemyev, A.V., Neishtadt, A.I., Vasiliev, A.A., Mourenas, D., 2017b. Phys. Rev. E 95, 023204. doi:10.1103/PhysRevE.95.023204.
- ¹⁶Artemyev, A.V., Neishtadt, A.I., Vasiliev, A.A., Mourenas, D., 2018b. Journal of Plasma Physics 84, 905840206. doi:10.1017/S0022377818000260.
- ¹⁷Artemyev, A.V., Neishtadt, A.I., Zelenyi, L.M., 2011. Chaos 21, 043120. doi:10.1063/1.3657916.
- ¹⁸Artemyev, A.V., Vasiliev, A.A., Mourenas, D., Agapitov, O., Krasnoselskikh, V., Boscher, D., Rolland, G., 2014a. Geophys. Res. Lett. 41, 5727–5733. doi:10.1002/2014GL061380.
- ¹⁹Artemyev, A.V., Vasiliev, A.A., Mourenas, D., Agapitov, O.V., Krasnoselskikh, V.V., 2014b. Physics of Plasmas 21, 102903. doi:10.1063/1.4897945.
- ²⁰Artemyev, A.V., Vasiliev, A.A., Mourenas, D., Neishtadt, A.I., Agapitov, O.V., Krasnoselskikh, V., 2015. Physics of Plasmas 22, 112903. doi:10.1063/1.4935842.
- ²¹Bell, T.F., 1984. J. Geophys. Res. 89, 905–918. doi:10.1029/JA089iA02p00905.
- ²²Bortnik, J., Thorne, R.M., Inan, U.S., 2008. Geophys. Res. Lett. 35, 21102. doi:10.1029/2008GL035500.
- ²³Cattell, C., Wygant, J.R., Goetz, K., Kersten, K., Kellogg, P.J., von Rosenvinge, T., Bale, S.D., Roth, I., Temerin, M., Hudson, M.K., Mewaldt, R.A., Wiedenbeck, M., Maksimovic, M., Ergun, R., Acuna, M., Russell, C.T., 2008. Geophys. Res. Lett. 35, 1105. doi:10.1029/2007GL032009.
- ²⁴Chirikov, B.V., 1979. Physics Reports 52, 263–379. doi:10.1016/0370-1573(79)90023-1.
- ²⁵Demekhov, A.G., Trakhtengerts, V.Y., Rycroft, M., Nunn, D., 2009. Geomagnetism and Aeronomy 49, 24–29. doi:10.1134/S0016793209010034.
- ²⁶Demekhov, A.G., Trakhtengerts, V.Y., Rycroft, M.J., Nunn, D., 2006. Geomagnetism and Aeronomy 46, 711–716. doi:10.1134/S0016793206060053.
- ²⁷Fu, X., Cowee, M.M., Friedel, R.H., Funsten, H.O., Gary, S.P., Hospodarsky, G.B., Kletzing, C., Kurth, W., Larsen, B.A., Liu, K., MacDonald, E.A., Min, K., Reeves, G.D., Skoug, R.M., Winske, D., 2014. Journal of Geophysical Research (Space Physics) 119, 8288–8298. doi:10.1002/2014JA020364.
- ²⁸Furuya, N., Omura, Y., Summers, D., 2008. J. Geophys. Res. 113, 4224. doi:10.1029/2007JA012478.
- ²⁹Gary, S.P., Wang, J., 1996. J. Geophys. Res. 101, 10749–10754. doi:10.1029/96JA00323.
- ³⁰Hsieh, Y.K., Omura, Y., 2017. J. Geophys. Res. 122, 675–694. doi:10.1002/2016JA023255.
- ³¹Hsieh, Y.K., Omura, Y., 2017. Radio Science 52, 1268–1281. URL: <http://dx.doi.org/10.1002/2017RS006245>, doi:10.1002/2017RS006245.
- ³²Itin, A.P., Neishtadt, A.I., Vasiliev, A.A., 2000. Physica D: Nonlinear Phenomena 141, 281–296. doi:10.1016/S0167-2789(00)00039-7.
- ³³Karpman, V.I., 1974. Space Sci. Rev. 16, 361–388. doi:10.1007/BF00171564.
- ³⁴Karpman, V.I., Istomin, J.N., Shklyar, D.R., 1974. Plasma Physics 16, 685–703. doi:10.1088/0032-1028/16/8/001.
- ³⁵Katoh, Y., Omura, Y., 2007a. Geophys. Res. Lett. 34, 3102.

- doi:10.1029/2006GL028594.
- ³⁶Katoh, Y., Omura, Y., 2007b. *Geophys. Res. Lett.* 34, L13102. doi:10.1029/2007GL029758.
- ³⁷Kennel, C.F., Engelmann, F., 1966. *Physics of Fluids* 9, 2377–2388. doi:10.1063/1.1761629.
- ³⁸Kennel, C.F., Wong, H.V., 1967. *Journal of Plasma Physics* 1, 75. doi:10.1017/S002237780000310X.
- ³⁹Khazanov, G.V., Tel'nikhin, A.A., Kronberg, T.K., 2013. *Journal of Geophysical Research (Space Physics)* 118, 6397–6404. doi:10.1002/2013JA019122.
- ⁴⁰Khazanov, G.V., Tel'nikhin, A.A., Kronberg, T.K., 2014. *Nonlinear Processes in Geophysics* 21, 61–85. doi:10.5194/npg-21-61-2014.
- ⁴¹Kitahara, M., Katoh, Y., 2019. *J. Geophys. Res.* 124, 5568–5583. doi:10.1029/2019JA026493.
- ⁴²Krafft, C., Volokitin, A.S., Flé, M., 2000. *Physics of Plasmas* 7, 4423–4432. doi:10.1063/1.1308565.
- ⁴³Kuzichev, I.V., Soto-Chavez, A.R., Park, J., Gerrard, A., Spitkovsky, A., 2019a. *Physics of Plasmas* 26, 072901. doi:10.1063/1.5096537.
- ⁴⁴Kuzichev, I.V., Vasko, I.Y., Rualdo Soto-Chavez, A., Tong, Y., Artemyev, A.V., Bale, S.D., Spitkovsky, A., 2019b. *Astrophys. J.* 882, 81. doi:10.3847/1538-4357/ab3290, arXiv:1907.04878.
- ⁴⁵Lerche, I., 1968 *Physics of Fluids* 11.
- ⁴⁶Li, W., Bortnik, J., Thorne, R.M., Angelopoulos, V., 2011. *J. Geophys. Res.* 116, 12205. doi:10.1029/2011JA017035.
- ⁴⁷Li, W., Bortnik, J., Thorne, R.M., Cully, C.M., Chen, L., Angelopoulos, V., Nishimura, Y., Tao, J.B., Bonnell, J.W., Lecontel, O., 2013. *J. Geophys. Res.* 118, 1461–1471. doi:10.1002/jgra.50176.
- ⁴⁸Li, W., Mourenas, D., Artemyev, A.V., Bortnik, J., Thorne, R.M., Kletzing, C.A., Kurth, W.S., Hospodarsky, G.B., Reeves, G.D., Funsten, H.O., Spence, H.E., 2016. *Geophys. Res. Lett.* 43, 8867–8875. doi:10.1002/2016GL070386.
- ⁴⁹Lichtenberg, A.J., Lieberman, M.A., 1983. Regular and stochastic motion.
- ⁵⁰Lyons, L.R., Williams, D.J., 1984. Quantitative aspects of magnetospheric physics.
- ⁵¹Mourenas, D., Artemyev, A.V., Agapitov, O.V., Krasnoselskikh, V., Mozer, F.S., 2015. *J. Geophys. Res.* 120, 3665–3683. doi:10.1002/2015JA021135.
- ⁵²Mourenas, D., Artemyev, A.V., Agapitov, O.V., Mozer, F.S., Krasnoselskikh, V.V., 2016. *J. Geophys. Res.* 121, 4498–4517. doi:10.1002/2015JA022223.
- ⁵³Mourenas, D., Zhang, X.J., Artemyev, A.V., Angelopoulos, V., Thorne, R.M., Bortnik, J., Neishtadt, A.I., Vasiliev, A.A., 2018. *J. Geophys. Res.* 123, 4979–4999. doi:10.1029/2018JA025417.
- ⁵⁴Neishtadt, A., 1975. *Journal of Applied Mathematics and Mechanics* 39, 594–605. doi:10.1016/0021-8928(75)90060-X.
- ⁵⁵Neishtadt, A.I., 1999. On Adiabatic Invariance in Two-Frequency Systems. in Hamiltonian Systems with Three or More Degrees of Freedom, ed. Simo C., NATO ASI Series C. Dordrecht: Kluwer Acad. Publ. 533, 193–213. doi:10.1063/1.166236.
- ⁵⁶Neishtadt, A.I., 2014. *Russian Mathematical Surveys* 69, 771. URL: <http://stacks.iop.org/0036-0279/69/i=5/a=771>.
- ⁵⁷Ni, B., Thorne, R.M., Zhang, X., Bortnik, J., Pu, Z., Xie, L., Hu, Z.j., Han, D., Shi, R., Zhou, C., Gu, X., 2016. Origins of the Earth's Diffuse Auroral Precipitation. *Space Sci. Rev.* 200, 205–259. doi:10.1007/s11214-016-0234-7.
- ⁵⁸Nunn, D., 1971. *Journal of Plasma Physics* 6, 291. doi:10.1017/S0022377800006061.
- ⁵⁹Nunn, D., Omura, Y., 2015. *J. Geophys. Res.* 120, 2890–2911. doi:10.1002/2014JA020898.
- ⁶⁰Omura, Y., Furuya, N., Summers, D., 2007. *J. Geophys. Res.* 112, 6236. doi:10.1029/2006JA012243.
- ⁶¹Omura, Y., Matsumoto, H., Nunn, D., Rycroft, M.J., 1991. *Journal of Atmospheric and Terrestrial Physics* 53, 351–368.
- ⁶²Omura, Y., Miyashita, Y., Yoshikawa, M., Summers, D., Hikishima, M., Ebihara, Y., Kubota, Y., 2015. *J. Geophys. Res.* 120, 9545–9562. doi:10.1002/2015JA021563.
- ⁶³Sagdeev, R.Z., Usikov, D.A., Zaslavsky, G.M., 1988. Nonlinear Physics. From the Pendulum to Turbulence and Chaos.
- ⁶⁴Shaaban, S.M., Lazar, M., Yoon, P.H., Poedts, S., López, R.A., 2019. *Monthly Notices of the Royal Astronomical Society* 486, 4498–4507. doi:10.1093/mnras/stz830, arXiv:1903.08005.
- ⁶⁵Shklyar, D.R., 1981. *Sov. Phys. JETP* 53, 1197–1192.
- ⁶⁶Shklyar, D.R., Matsumoto, H., 2009. *Surveys in Geophysics* 30, 55–104. doi:10.1007/s10712-009-9061-7.
- ⁶⁷Shprits, Y.Y., Subbotin, D.A., Meredith, N.P., Elkington, S.R., 2008. *Journal of Atmospheric and Solar-Terrestrial Physics* 70, 1694–1713. doi:10.1016/j.jastp.2008.06.014.
- ⁶⁸Solovev, V.V., Shkliar, D.R., 1986. *Sov. Phys. JETP* 63, 272–277.
- ⁶⁹Stenzel, R.L., 1999. *J. Geophys. Res.* 104, 14379–14396. doi:10.1029/1998JA900120.
- ⁷⁰Stix, T.H., 1962. *The Theory of Plasma Waves*.
- ⁷¹Summers, D., Thorne, R.M., Xiao, F., 1998. *J. Geophys. Res.* 103, 20487–20500. doi:10.1029/98JA01740.
- ⁷²Tao, X., Bortnik, J., Albert, J.M., Thorne, R.M., 2012a. *J. Geophys. Res.* 117, 10205. doi:10.1029/2012JA017931.
- ⁷³Tao, X., Bortnik, J., Thorne, R.M., Albert, J.M., Li, W., 2012b. *Geophys. Res. Lett.* 39, 6102. doi:10.1029/2012GL051202.
- ⁷⁴Tao, X., Chen, L., Liu, X., Lu, Q., Wang, S., 2017a. *Geophysical Research Letters* URL: <http://dx.doi.org/10.1002/2017GL074881>, doi:10.1002/2017GL074881.
- ⁷⁵Tao, X., Zonca, F., Chen, L., 2017b. *Geophys. Res. Lett.* 44, 3441–3446. URL: <http://dx.doi.org/10.1002/2017GL072624>, doi:10.1002/2017GL072624.
- ⁷⁶Thorne, R.M., 2010. *Geophys. Res. Lett.* 372, 22107. doi:10.1029/2010GL044990.
- ⁷⁷Thorne, R.M., Li, W., Ni, B., Ma, Q., Bortnik, J., Chen, L., Baker, D.N., Spence, H.E., Reeves, G.D., Henderson, M.G., Kletzing, C.A., Kurth, W.S., Hospodarsky, G.B., Blake, J.B., Fenner, J.F., Claudepierre, S.G., Kanekal, S.G., 2013. *Nature* 504, 411–414. doi:10.1038/nature12889.
- ⁷⁸Thorne, R.M., Ni, B., Tao, X., Horne, R.B., Meredith, N.P., 2010. *Nature* 467, 943–946. doi:10.1038/nature09467.
- ⁷⁹Titova, E.E., Kozelov, B.V., Jiricek, F., Smilauer, J., Demekhov, A.G., Trakhtengerts, V.Y., 2003. *Annales Geophysicae* 21, 1073–1081. doi:10.5194/angeo-21-1073-2003.
- ⁸⁰Tong, Y., Vasko, I.Y., Artemyev, A.V., Bale, S.D., Mozer, F.S., 2019. *Astrophys. J.* 878, 41. doi:10.3847/1538-4357/ab1f05, arXiv:1905.08958.
- ⁸¹Tyler, E., Breneman, A., Cattell, C., Wygant, J., Thaller, S., Malaspina, D., 2019. *Geophys. Res. Lett.* 46, 2328–2336. doi:10.1029/2019GL082292.
- ⁸²Vainchtein, D., Zhang, X.J., Artemyev, A., Mourenas, D., Angelopoulos, V., Thorne, R.M., 2018. *J. Geophys. Res.* doi:10.1029/2018ja025654.
- ⁸³Van Compernolle, B., An, X., Bortnik, J., Thorne, R.M., Pribyl, P., Gekelman, W., 2015. *Physical Review Letters* 114, 245002. doi:10.1103/PhysRevLett.114.245002.
- ⁸⁴Van Kampen, N.G., 2003. *Stochastic Processes in Physics and Chemistry*. 3 ed., North Holland.
- ⁸⁵Vasiliev, A., Neishtadt, A., Artemyev, A., 2011. *Physics Letters A* 375, 3075–3079. doi:10.1016/j.physleta.2011.06.055.
- ⁸⁶Vasko, I.Y., Mozer, F.S., Krasnoselskikh, V.V., Artemyev, A.V., Agapitov, O.V., Bale, S.D., Avanov, L., Ergun, R., Giles, B., Lindqvist, P.A., Russell, C.T., Strangeway, R., Torbert, R., 2018. *Geophys. Res. Lett.* 45, 5809–5817. doi:10.1029/2018GL077835.
- ⁸⁷Vedenov, A.A., Sagdeev, R.Z., 1961. Some properties of a plasma with an anisotropic ion velocity distribution in a magnetic field, in: Leontovich, M.A. (Ed.), *Plasma Physics and the Problem of Controlled Thermonuclear Reactions*, Volume 3, p. 332.
- ⁸⁸Vedenov, A.A., Velikhov, E., Sagdeev, R., 1962. Quasilinear theory of plasma oscillations. *Nuclear Fusion Suppl.* 2, 465–475.
- ⁸⁹Veltri, P., Mangeney, A., Scudder, J.D., 1992. *Nuovo Cimento C Geophysics Space Physics* C 15, 607–619. doi:10.1007/BF02507834.
- ⁹⁰Veltri, P., Zimbardo, G., 1993. *J. Geophys. Res.* 98, 13335–13346. doi:10.1029/93JA01144.

- ⁹¹Volokitin, A.S., Krafft, C., 2001a. Physics of Plasmas 8, 3748–3758. doi:10.1063/1.1380694.
- ⁹²Volokitin, A.S., Krafft, C., 2001b. Physics of Plasmas 8, 4960–4971. doi:10.1063/1.1398085.
- ⁹³Wilson, III, L.B., Cattell, C.A., Kellogg, P.J., Wygant, J.R., Goetz, K., Breneman, A., Kersten, K., 2011. Geophys. Res. Lett. 38, 17107. doi:10.1029/2011GL048671.
- ⁹⁴Wilson, III, L.B., Koval, A., Szabo, A., Breneman, A., Cattell, C.A., Goetz, K., Kellogg, P.J., Kersten, K., Kasper, J.C., Maruca, B.A., Pulupa, M., 2012. Geophys. Res. Lett. 39, 8109. doi:10.1029/2012GL051581.
- ⁹⁵Yoon, P.H., Pandey, V.S., Lee, D.H., 2013. Physics of Plasmas 20, 112902. doi:10.1063/1.4831965.
- ⁹⁶Zhang, X., Angelopoulos, V., Artemyev, A.V., Liu, J., 2018a. Geophys. Res. Lett. 45, 9380–9389. doi:10.1029/2018GL079613.
- ⁹⁷Zhang, X.J., Mourenas, D., Artemyev, A.V., Angelopoulos, V., Bortnik, J., Thorne, R.M., Kurth, W.S., Kletzing, C.A., Hospodarsky, G.B., 2019. Geophysical Research Letters 46, 7182–7190. URL: <https://agupubs.onlinelibrary.wiley.com/doi/abs/10.1029/2019GL083833>, doi:10.1029/2019GL083833,
- ⁹⁸Zhang, X.J., Thorne, R., Artemyev, A., Mourenas, D., Angelopoulos, V., Bortnik, J., Kletzing, C.A., Kurth, W.S., Hospodarsky, G.B., 2018b. J. Geophys. Res. 123, 5379–5393. URL: <https://agupubs.onlinelibrary.wiley.com/doi/abs/10.1029/2018JA025390>, doi:10.1029/2018JA025390,